Spatio-Temporal Delta-Sigma Modulation for Shared Wideband Transmit Arrays

Dan P. Scholnik and Jeffrey O. Coleman
Radar Division, Naval Research Laboratory
Washington, DC
scholnik@nrl.navy.mil, jeffrey.coleman@nrl.navy.mil

Donald Bowling and Michael Neel
Naval Air Warfare Center
China Lake, CA
donald.bowling@navy.mil, michael.neel@nrl.navy.mil

***Abstract*— Future array-based RF transmit systems will require linear amplification to preserve the spectral integrity of simultaneously transmitted signals. Classical delta-sigma modulation, paired with an emerging class of high-power switches, can provide this linearity by using a high-speed, low-resolution quantizer and shaping the resulting quantization errors out of the signal band. The drawback is that high clock rates are required to achieve high SNR. Recently we have proposed jointly shaping quantization errors in temporal and spatial frequency, pushing quantization errors both out of band and to nonpropagating spatial frequencies. This provides greater SNR for a given clock rate or the same SNR at a reduced clock rate relative to conventional delta-sigma modulation, while retaining its characteristic high linearity. In this paper we present an overview of the spatio-temporal delta-sigma array architecture and present the results of some preliminary hardware experiments with a small linear array.**

I. Introduction

Delta-sigma ($\Delta\Sigma$) modulation is widely used in D/A and A/D conversion to obtain high precision, linearity, and dynamic range in exchange for a higher sampling rate or lower bandwidth [1] by placing a low-resolution quantizer inside a feedback loop to spectrally shape quantization noise to minimize its interference with the signal. Out-of-band quantization noise is then removed with digital or analog filtering according to the application (A/D or D/A). High oversampling rates (clock rates relative to signal bandwidths) result in signal-to-noise ratio (SNR) levels often exceeding the roughly 100 dB limit of conventional (Nyquist-rate) converters. One-bit quantizers have traditionally been used for their automatically near-ideal characteristics, but newer multi-bit $\Delta\Sigma$-like architectures [2]–[4] based on dynamic element matching (DEM) spectrally shape hardware-mismatch errors as well and lower oversampling requirements by increasing parallelism [5].

Spatial multidimensional $\Delta\Sigma$ modulation of images to produce halftone images from continuous-tone ones is known as *error diffusion* [6], [7]. Typically, continuous-valued image files viewed on a monitor at 100 dots per inch (DPI) are converted to 600+ DPI binary-valued images for printing. Single-bit quantizers are used here not because they are ideal, but because they model printers and displays with binary-valued pixels. The inherent lowpass nature of human vision then replaces the explicit post-modulator filtering that removes quantization noise in temporal $\Delta\Sigma$ modulation.

Given the benefits of temporal and spatial $\Delta\Sigma$ modulators individually, it is natural to consider a joint space-time $\Delta\Sigma$ modulator [8]–[10]. The primary application of interest is to digitally controlled transmit arrays of medium to high bandwidth for RF systems in which hardware simplicity and near-perfect amplifier linearity make single-bit outputs attractive. A new class of high-speed, high-power RF switches have been proposed [11] for this application. We present in section II a space-time $\Delta\Sigma$ modulation architecture that jointly shapes the quantization noise in both temporal and spatial frequency. By oversampling spatially and exploiting the bandpass nature of wave propagation, temporal oversampling requirements can be reduced.

This work was supported by the Office of Naval Research.

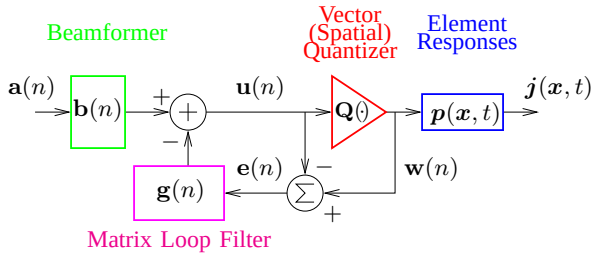

Fig. 1. Spatio-temporal $\Delta\Sigma$ modulator.

Recently we conducted preliminary hardware experiments aimed at demonstrating joint spatio-temporal quantization noise shaping and its advantages over conventional temporal-only modulation. An overview of the experiments and some key results are presented in section III.

II. System Description

A. Input-Output Relationship

The proposed architecture for space-time $\Delta\Sigma$ modulation is shown in Fig. 1. The $N \times 1$ discrete-time input vector $\mathbf{a}(n)$ contains the N individual waveforms to be transmitted, while the columns of $K \times N$ matrix $\mathbf{b}(n)$ act as individual beamformers to generate K individual array-element drive signals. Each vector coordinate inside the $\Delta\Sigma$ loop corresponds to a hardware *unit element*, perhaps a high-power switch feeding a radiator in the array. We associate coordinate k with the spatial location $\mathbf{x}_k$ of the physical element. The loop is closed around the matrix loop filter $\mathbf{g}(n)$ operating on the quantization error $\mathbf{e}(n)$ of the vector (spatial) quantizer. The quantizer output is then the $\Delta\Sigma$-modulated space-time signal fed to the array. Analog responses and the physical radiators are modeled by the $L \times K$ matrix unit-sample response $\boldsymbol{p}(\boldsymbol{x},t)$, where L is

the number of dimensions to which the current density is restricted. The array output is the current density $\boldsymbol{j}(\boldsymbol{x},t)$.

Begin the analysis of Fig. 1 with the quantizer input,

$$\mathbf{u}(n) = (\mathbf{b} * \mathbf{a})(n) - (\mathbf{g} * \mathbf{e})(n).$$

Here $*$ indicates discrete-time matrix-vector convolution:

$$(\mathbf{b} * \mathbf{a})(n) \triangleq \sum_k \mathbf{b}(n-k)\mathbf{a}(k).$$

The quantizer output $\mathbf{w}(n) = \mathbf{u}(n) + \mathbf{e}(n)$ is then

$$\mathbf{w}(n) = (\mathbf{b} * \mathbf{a})(n) + (\mathbf{h} * \mathbf{e})(n),$$

where $\mathbf{h}(n) \triangleq \delta(n)\mathbf{I} - \mathbf{g}(n)$. Defining a temporal convolution in continuous/discrete-time by

$$(\boldsymbol{p} \star \mathbf{w})(\boldsymbol{x},t) \triangleq T \sum_k \boldsymbol{p}(\boldsymbol{x}, t-kT)\, \mathbf{w}(k),$$

where T is the discrete-time sample interval, yields the output of the individual radiators, before and after Fourier transforming on t, as

$$\begin{aligned} \boldsymbol{j}(\boldsymbol{x},t) &= \big(\boldsymbol{p} \star \mathbf{b} * \mathbf{a}\big)(\boldsymbol{x},t) \\ &\quad + \big(\boldsymbol{p} \star \mathbf{h} * \mathbf{e}\big)(\boldsymbol{x},t) \end{aligned} \tag{1}$$

$$\begin{aligned} \boldsymbol{J}(\boldsymbol{x},f) &= \boldsymbol{P}(\boldsymbol{x},f)\, T\mathbf{B}(fT)\, \mathbf{A}(fT) \\ &\quad + \boldsymbol{P}(\boldsymbol{x},f)\, T\mathbf{H}(fT)\, \mathbf{E}(fT). \end{aligned} \tag{2}$$

On the right in each the first and second terms are the desired signal and the quantization error respectively, each shaped by the pulse matrix after filtering. The goal is to minimize the effects of the quantization error in the region of the spatio-temporal spectrum that is occupied by the signal. The geometry of that region is the subject of the next section.

B. Far-Field Propagation as Spatial Filtering

The spatial and temporal output of the array is given in (1) in terms of the current density $\boldsymbol{j}$. We are ultimately interested in the corresponding far-field array response, which can be found by solving Maxwell's equations. We use the method of [12], first solving for the complex vector potential $\boldsymbol{\mathcal{A}}$, and then finding the complex electric field $\boldsymbol{\mathcal{E}}$ in the far field as

$$\boldsymbol{\mathcal{E}}(\boldsymbol{x},f) \approx -\mathrm{j}2\pi f \boldsymbol{\Gamma}_u \boldsymbol{\mathcal{A}}(\boldsymbol{x},f), \tag{3}$$

where $\boldsymbol{\Gamma}_u$ is the matrix that projects onto the plane perpendicular to direction vector $\boldsymbol{u} = \boldsymbol{x}/\|\boldsymbol{x}\|$. The far-field, for purposes of this paper, will be somewhat loosely defined as $\|\boldsymbol{x}\|$ large with respect to the size of the array.

The vector potential $\boldsymbol{\mathcal{A}}$ represents a weighted spherical wave propagating away from each point on the antenna at a speed c, which is represented mathematically as a convolution in $\boldsymbol{x}$ of the current density with a spherical wave centered at the origin:

$$\boldsymbol{\mathcal{A}}(\boldsymbol{x},f) = \frac{\mu}{4\pi} \int \frac{e^{-\mathrm{j}2\pi\|\boldsymbol{x}-\boldsymbol{x}'\|f/c}}{\|\boldsymbol{x}-\boldsymbol{x}'\|} \boldsymbol{J}(\boldsymbol{x}',f)\, d\boldsymbol{x}'. \tag{4}$$

In the far field, this is approximately

$$\boldsymbol{\mathcal{A}}(\boldsymbol{x},f) \approx \frac{\mu e^{-\mathrm{j}2\pi\|\boldsymbol{x}\|f/c}}{4\pi\|\boldsymbol{x}\|} \mathbf{J}(-\boldsymbol{u}f/c, f). \tag{5}$$

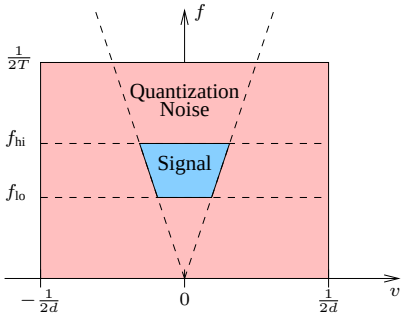

Fig. 2. Spatio-temporal spectral regions.

Thus the far-field vector potential in the direction $\boldsymbol{u}$ resulting from any current density $\boldsymbol{j}$ is just a spherical wave weighted by the spatio-temporal Fourier transform $\mathbf{J}(\boldsymbol{v},f)$ of the current density evaluated at $\boldsymbol{v} = -\boldsymbol{u}f/c$. As a consequence of the far-field assumption the dependence on distance $\|\boldsymbol{x}\|$ and direction $\boldsymbol{u}$ have been completely decoupled. The corresponding complex electric field $\boldsymbol{\mathcal{E}}$ for far-field $\boldsymbol{x}$ is found via (3):

$$\boldsymbol{\mathcal{E}}(\boldsymbol{x},f) \approx -\frac{\mu e^{-\mathrm{j}2\pi\|\boldsymbol{x}\|f/c}}{4\pi\|\boldsymbol{x}\|} \mathrm{j}2\pi f \boldsymbol{\Gamma}_u \mathbf{J}(-\boldsymbol{u}f/c, f). \tag{6}$$

In (6) we see that the dependence of the far-field electric field on the 4D Fourier transform $\mathbf{J}(\boldsymbol{v},f)$ of the current density is limited to spatial and temporal frequencies such that $\boldsymbol{v} = -\boldsymbol{u}f/c$, or equivalently $\|\boldsymbol{v}\| = |f|/c$. This is a version of the Helmholtz equation, specifying which spatio-temporal frequencies can propagate into the far-field. We will refer to this set of propagating frequencies as the *Helmholtz cone*. Spatio-temporal frequencies not on the cone are effectively filtered out by far-field propagation, and in this way the array itself serves as an output filter of the $\Delta\Sigma$ modulator.

If we consider only a single spatial dimension and corresponding spatial frequency v (appropriate for array elements on a line), then the projection of the cone into the (v,f) plane shown in Fig. 2 suggests how to choose the noise shaping in a space-time $\Delta\Sigma$ modulator. The center trapezoid is the intersection of the temporal frequency band of interest and the cone and represents the spectral support of the desired signal where quantization noise should be suppressed. The surrounding region then holds the shaped quantization errors. The shaded rectangle represents one possible spatio-temporal region over which we have independent control of the noise shaping. It represents the positive-frequency half of one period of the 2D frequency response of the column noise transfer functions (defined in the next section) when the sampling interval is T and the element spacing is d.

C. Noise Transfer Function

We now examine in more detail the responses that modify the quantization noise in (2). Writing the kth column of $\boldsymbol{P}(\boldsymbol{x},f)$ as $\boldsymbol{P}_k(\boldsymbol{x}-\mathbf{x}_k,f)$ to indicate its spatial offset, the error-signal (second) term of (2) becomes

$$\boldsymbol{J}_e(\boldsymbol{x},f) = \sum_n E_n(fT) \sum_k \boldsymbol{P}_k(\boldsymbol{x}-\mathbf{x}_k,f) T H_{k,n}(fT).$$

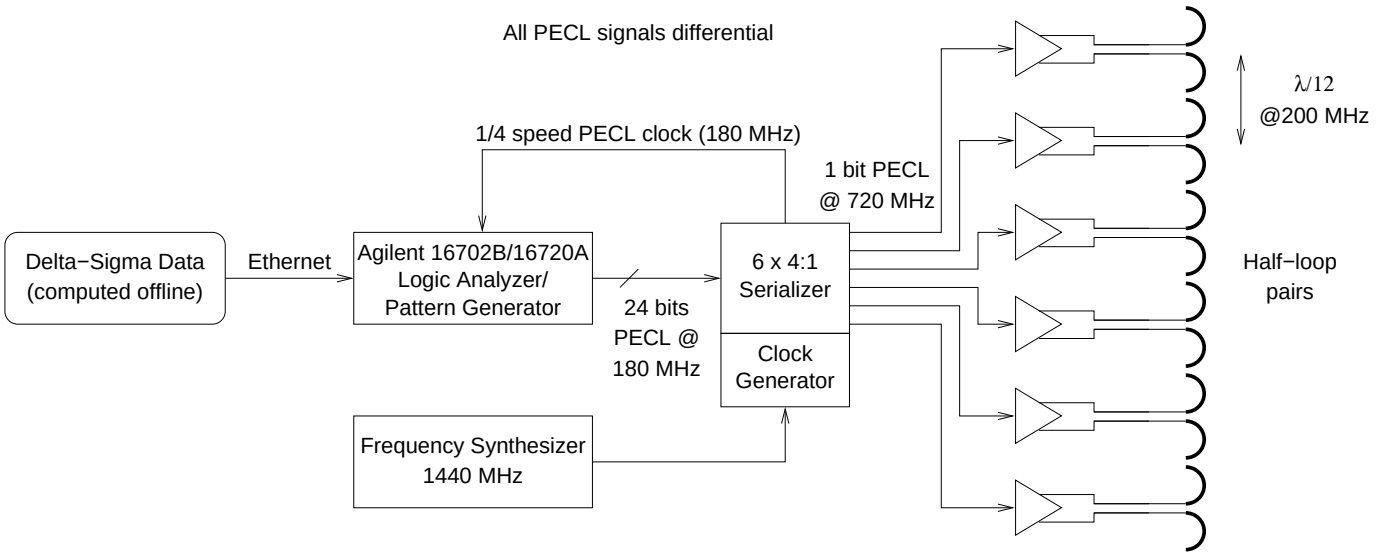

Fig. 3. Transmit-side hardware setup used in experiments.

Fourier transforming on $\boldsymbol{x}$ yields

$$\mathbf{J}_e(\boldsymbol{v},f)=\sum_n E_n(fT)\sum_k \mathbf{P}_k(\boldsymbol{v},f)TH_{k,n}(fT)e^{-\mathrm{j}2\pi\mathbf{x}_k^T\boldsymbol{v}} \tag{7}$$

for arbitrary element responses and

$$\mathbf{J}_e(\boldsymbol{v},f) = \mathbf{P}_0(\boldsymbol{v},f)T\sum_n \mathrm{H}_n(\boldsymbol{v},fT)E_n(fT) \tag{8}$$

for identical elements. Column *noise transfer function* (NTF) $\mathrm{H}_n(\boldsymbol{v},fT)$ is the spatial and temporal shaping applied to element $E_n(fT)$ of the quantization error.

Substituting (7) or (8) into (6) yields the electric field due to far-field quantization noise $\boldsymbol{\mathcal{E}}_e(\boldsymbol{x},f)$. Typically we wish to minimize the total far-field noise power (found by integrating $|\boldsymbol{\mathcal{E}}_e(\boldsymbol{x},f)|^2$ over a far-field spherical shell) in a given band of temporal frequencies, subject to computability constraints on the structure of the loop filter and stability constraints on the out-of-band noise gain. If we assume that the individual error vector elements are white and uncorrelated with each other, then this problem reduces down to the independent design of the N columns of $\mathbf{h}(n)$. If $\mathbf{h}(n)$ is FIR, then the optimization is convex and can be efficiently solved using second-order cone programming or similar convex quadratic methods. Loop filter design is considered in more detail in [9], [10].

III. A Six-Element Hardware Experiment

Recently some preliminary hardware experiments were performed, with the primary goal to demonstrate the ability to shape the quantization noise of a transmit array in both spatial and temporal frequency. A secondary goal was to show the flexibility of a simple array driven by binary signals by transmitting multiple signals on independent beams and frequencies. High performance (in terms of SNR or efficiency) was neither expected nor achieved, and we instead focused on high bandwidths (relative to the sampling rate and RF frequency) and correspondingly low temporal oversampling ratios.

A. Experimental Setup

The transmit side of the test setup used for most of the experiments is shown in Fig. 3. Digital waveforms were generated offline using Matlab-based software and uploaded to an Agilent pattern generator that can store up to 16M 24-bit words. We used 24 bit differential positive emitter-coupled logic (PECL) outputs at 180 MHz to drive six 4:1 serializers on a custom board, which then output six 720 MHz PECL bit streams. The six differential bitstreams were amplified by a pair of AC-coupled op-amps which in turn drove the array elements. The transmit array was made up of pairs of square half-loops as shown in Figures 4 and 5. Six active pairs with a guard pair at each end were mounted on a 48" by 48" ground plane. The element spacing in the array was approximately $\lambda/12$ at the nominal operating frequency of 200 MHz, for a spatial oversampling ratio (OSR) of 6. At this frequency the elements are electrically small and show little mutual coupling. The nominal bandwidth used was 200 MHz, corresponding to a temporal OSR of 1.8. This is much lower than conventional $\Delta\Sigma$ modulators are typically designed for, and allows us to demonstrate how spatio-temporal $\Delta\Sigma$ modulation can improve SNR in a spatially oversampled array even in the absence of significant temporal oversampling.

The receive test setup was made as simple as possible: a low-gain (2.5 dB) biconical dipole antenna (shown in Fig. 6) in the far field feeding an LNA and an HP spectrum analyzer. As the received power was quite small, the LNA was required to boost the signals above the analyzer noise floor. The low received power also precluded the use of high temporal oversampling ratios, as the resulting shaped quantization noise floor would lie below thermal noise.

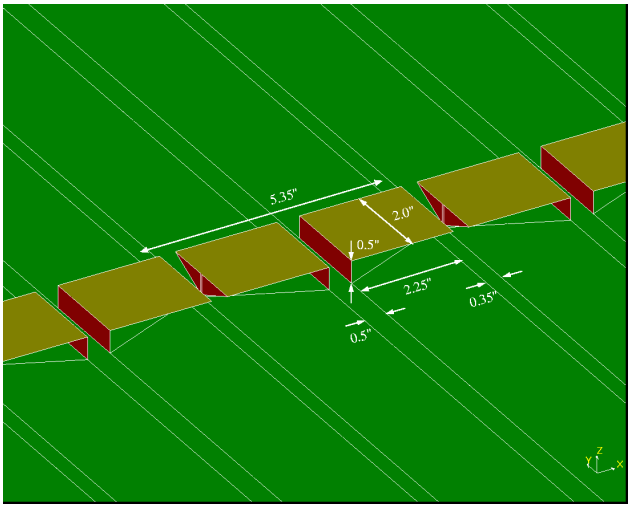

Fig. 4. The spatially oversampled dual half-loop array geometry.

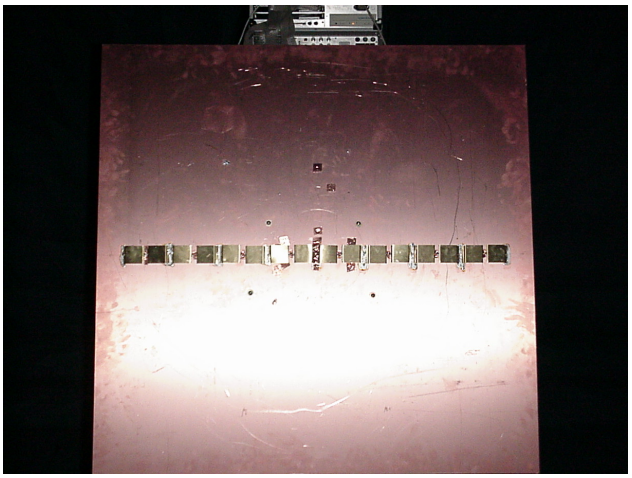

Fig. 5. The array face.

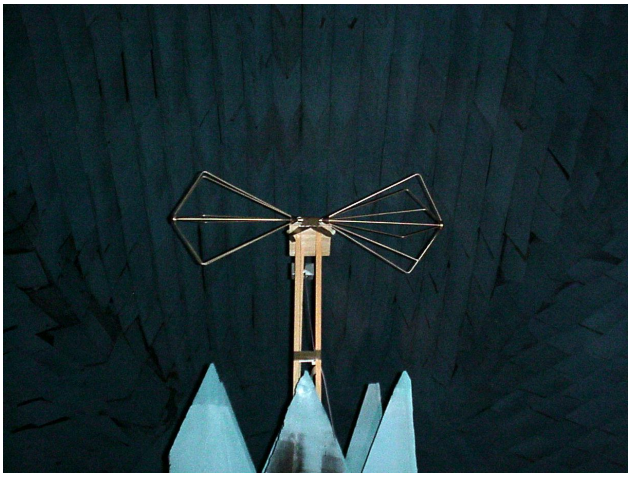

Fig. 6. The biconical receive antenna.

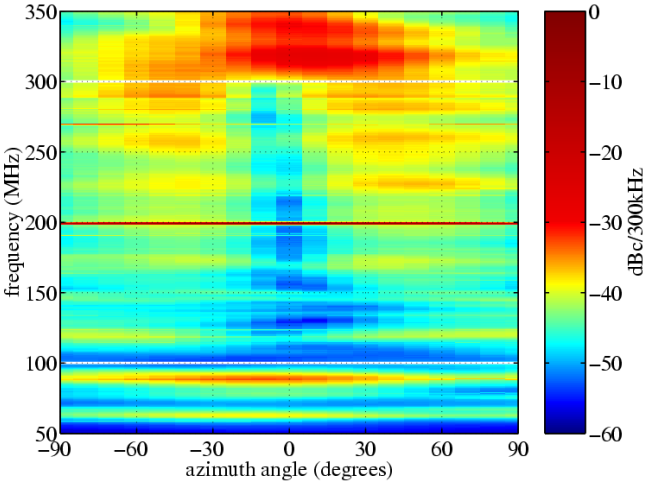

(a) Narrow noise notch at 0°

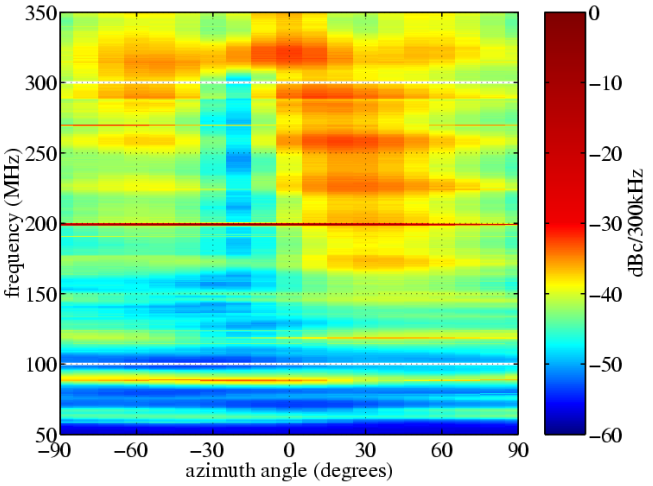

(b) Narrow noise notch at -30°

Fig. 7. Power spectra of received spatio-temporal $\Delta\Sigma$-modulated signal with a noise notch at a single angle.

B. Test Results

In most practical systems, we wish to suppress in-band quantization noise for all visible angles. It is illustrative, however, to first design a loop filter that only minimizes quantization noise at a single angle. This was done for both boresight and -30°, with the received power spectra of a modulated 201 MHz sinusoid shown in Fig. 7. In both cases the temporal frequency range of the noise notch is 100 MHz to 300 MHz. A slight understeering effect can be seen due to the small ground plane; more on this later. Although it is difficult to produce a narrow notch with just six elements, it is clearly visible in both plots. Compare this to Fig. 8(b), where the quantization noise has been suppressed more-or-less evenly across all angles.

A logical point of comparison for single-bit spatio-temporal $\Delta\Sigma$ modulation is a set of identical but independent single-bit temporal-only $\Delta\Sigma$ modulators, one per element. Both use

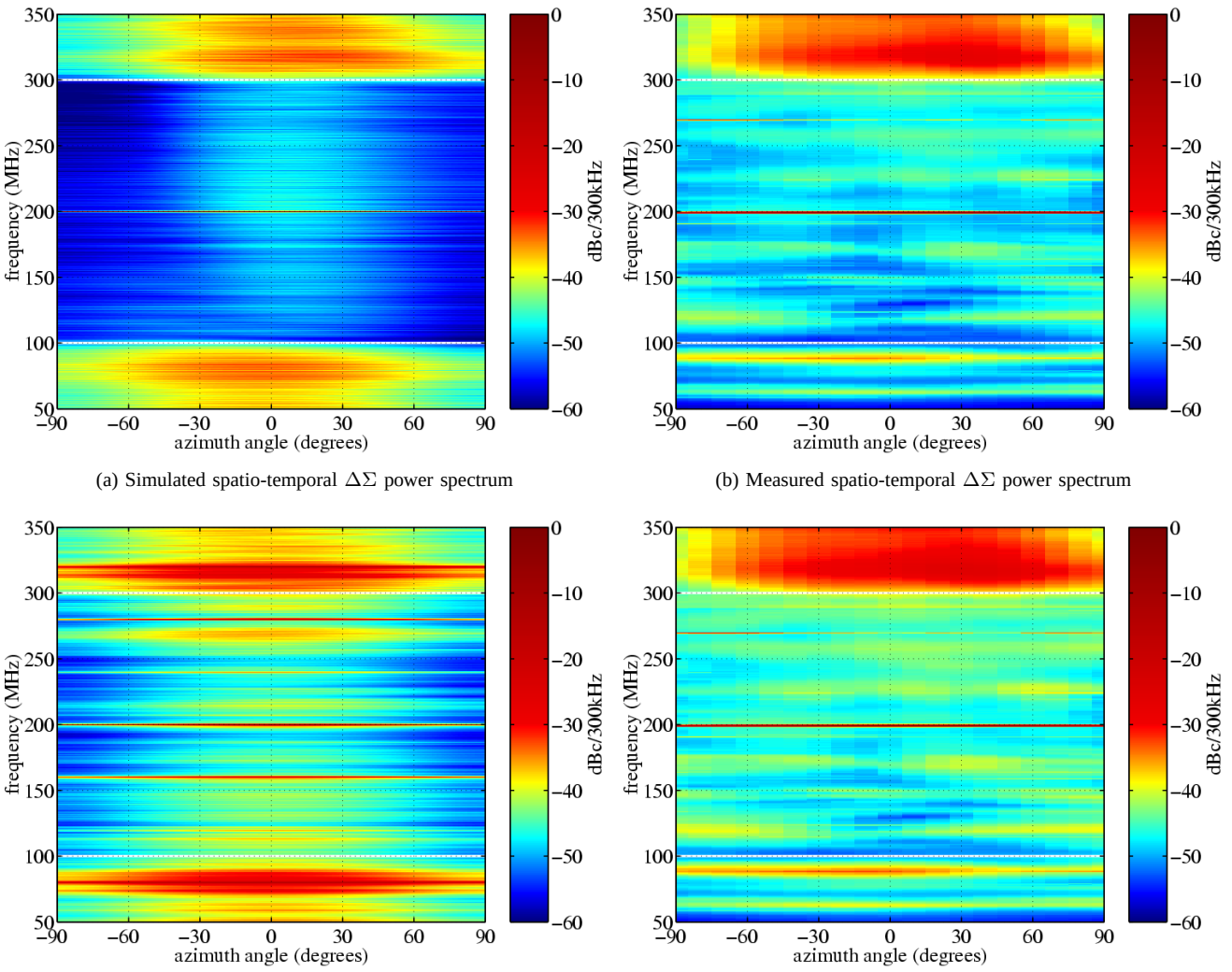

(a) Simulated spatio-temporal $\Delta\Sigma$ power spectrum

(b) Measured spatio-temporal $\Delta\Sigma$ power spectrum

(c) Simulated temporal-only $\Delta\Sigma$ power spectrum

(d) Measured temporal-only $\Delta\Sigma$ power spectrum

Fig. 8. Simulated and measured power spectra for spatio-temporal and conventional temporal-only $\Delta\Sigma$ modulation of a 201 MHz sinusoid within a 200 MHz wide noise notch.

the same hardware, but only the former can take advantage of spatial oversampling to improve SNR. Identical 201 MHz boresight beams were modulated using both methods, with equal-length loop filters designed to provide a noise notch from 100 MHz to 300 MHz (over all visible angles in the space-time case). Simulated and measured power spectra are shown in Fig. 8. A comparison of simulated and measured SNR is shown in Fig. 9. Enforcing spatial as well as temporal noise shaping with just six elements has gained over 8 dB of SNR. The measured SNR curves fall off faster with angle than predicted by simulation, as the shaped quantization noise at higher angles is increasingly dominated by interference (a consequence of the low received power levels).

To demonstrate the multifunction capability of such a digitally controlled array, seven sinusoids of different frequencies centered at 200 MHz were transmitted in seven different directions. The resulting patterns are shown in Fig. 10(a). Note again the strong understeering effect, seemingly limiting the possible scan directions to 30° or so. We attribute this to the relatively small ground plane used, which was confirmed by electromagnetic simulation. To demonstrate the frequency agility of the array, we repeated the experiment in the second Nyquist band, with beams spanning from 400 to 600 MHz (Fig. 10(b)). As the ground plane was in this case electrically larger, the understeering effect was somewhat less pronounced.

IV. Outstanding Issues

To date, several major research initiatives stand between this work and practical multifunction RF systems based on spatio-temporal $\Delta\Sigma$ modulation. On the analog hardware side, the issue is how to efficiently generate, filter, and radiate the single-bit signals. Although some work has been done of late on creating high-speed, high-efficiency class D/E/S switching amplifiers [11], the loads assumed typically look nothing like an array element. Small, tightly-packed elements tend to present highly reactive impedances to the driver, posing a great

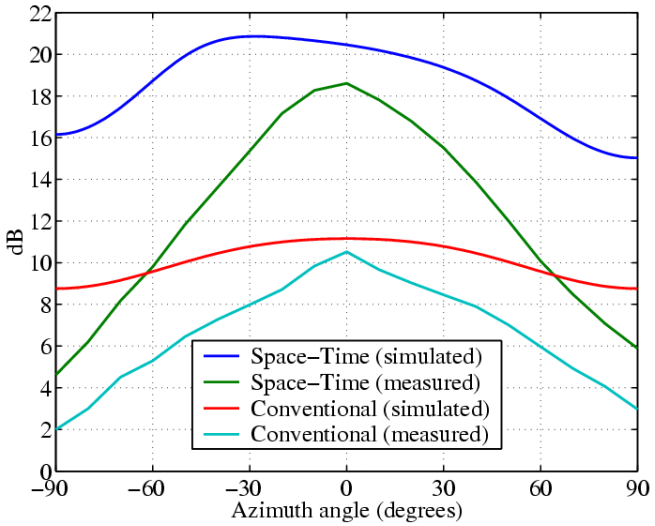

Fig. 9. Simulated and measured SNR for spatio-temporal and conventional temporal-only $\Delta\Sigma$ modulation of a 201 MHz sinusoid within a 200 MHz wide noise notch.

challenge to efficiency. On the digital side the fundamentals are better understood, but the challenge remains to efficiently implement a truly massive amount of potentially real-time computation.

REFERENCES

[1] J. C. Candy and G. C. Temes, "Oversampling methods for A/D and D/A conversion," in *Oversampled Delta-Sigma Data Converters*. New York: IEEE Press, 1991.

[2] R. Schreier and B. Zhang, "Noise-shaped multibit D/A converter employing unit elements," *Electronics Letters*, vol. 31, no. 20, pp. 1712–1713, Sept. 1995.

[3] I. Galton, "Spectral shaping of circuit errors in digital-to-analog converters," *IEEE Trans. Circuits and Systems II*, vol. 44, no. 10, pp. 808–817, Oct. 1997.

[4] D. P. Scholnik and J. O. Coleman, "Joint shaping of quantization and hardware-mismatch errors in a multibit delta-sigma DAC," in *Proc. 2000 Midwest Symp. on Circuits and Systems (MWSCAS 2000)*, Lansing MI, Aug. 2000.

[5] D. P. Scholnik, "A Parallel Digital Architecture for Delta-Sigma Modulation," in *Proc. 2002 Midwest Symp. on Circuits and Systems (MWSCAS 2002)*, Tulsa, OK, Aug. 2002.

[6] R. Floyd and L. Steinberg, "An adaptive algorithm for spatial grayscale," *Proc. Soc. Image Display*, vol. 17, no. 2, pp. 75–77, 1976.

[7] T. D. Kite, B. L. Evans, A. C. Bovik, and T. L. Sculley, "Digital halftoning as 2-D delta-sigma modulation," in *Proc. IEEE Int. Conf. Image Processing*, 1997, pp. 799–802.

[8] D. P. Scholnik and J. O. Coleman, "Joint Spatial and Temporal Delta-Sigma Modulation for Wideband Antenna Arrays and Video Halftoning," in *Proc. IEEE Int. Conf. Acoustic, Speech, and Signal Processing (ICASSP 2001)*, Salt Lake City, UT, May 2001.

[9] ——, "Computability Constraints in Space-Time Delta-Sigma Arrays," in *Proc. Asilomar Conf. on Signals, Systems, and Computers*, Pacific Grove, CA, Nov. 2001.

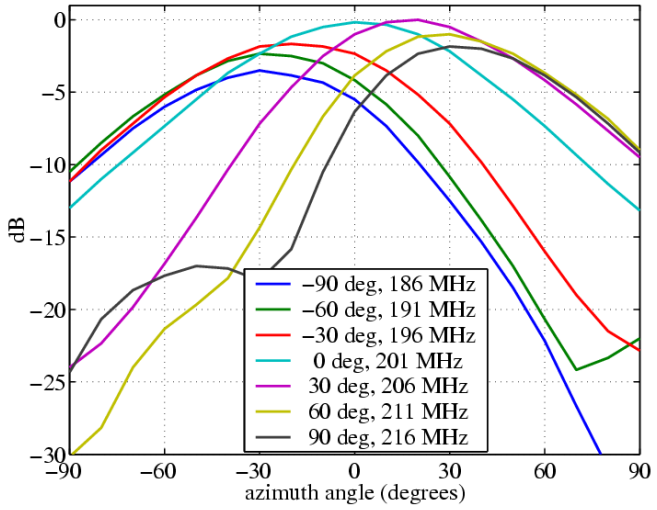

(a) Seven simultaneous beams, first Nyquist band

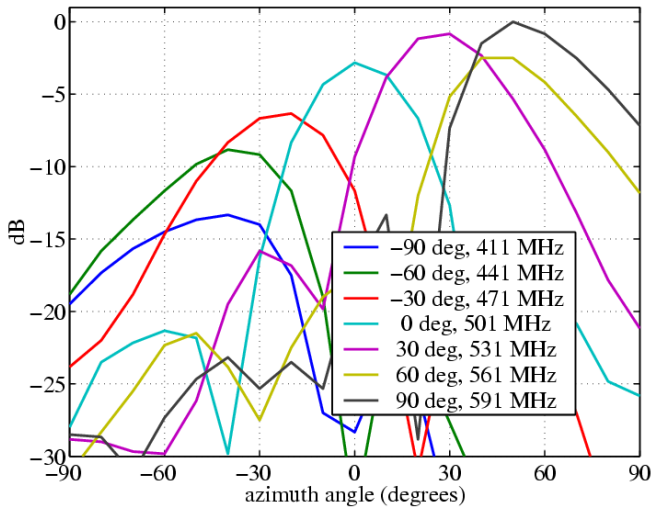

(b) Seven simultaneous beams, second Nyquist band

Fig. 10. Measured array patterns for multiple simultaneous beams in first and second Nyquist band.

[10] ——, "Space-Time Vector Delta-Sigma Modulation," in *Proc. 2002 Int'l Symp. on Circuits and Systems (ISCAS 2002)*, Scottsdale, AZ, May 2002.

[11] M. Iwamoto, A. Jayaraman, G. Hanington, P. Chen, A. Bellora, W. Thornton, L. Larson, and P. Asbeck, "Bandpass delta-sigma class-S amplifier," *Electronics Letters*, vol. 36, no. 12, pp. 1010–1012, June 2000.

[12] C. A. Balanis, *Antenna Theory*. John Wiley & Sons, Inc., 1982.